PCCP

PAPER

View Article Online
View Journal | View Issue

Cite this: *Phys. Chem. Chem. Phys.*, 2016, **18**, 29147

Competition between quasi-planar and cage-like structures in the B_{29}^- cluster: photoelectron spectroscopy and *ab initio* calculations†

Hai-Ru Li,[a] Tian Jian,[b] Wei-Li Li,[b] Chang-Qing Miao,[c] Ying-Jin Wang,[a] Qiang Chen,[ac] Xue-Mei Luo,[a] Kang Wang,[a] Hua-Jin Zhai,*[ad] Si-Dian Li*[a] and Lai-Sheng Wang*[b]

Received 4th August 2016,
Accepted 23rd September 2016

DOI: 10.1039/c6cp05420j

www.rsc.org/pccp

Size-selected boron clusters have been found to be predominantly planar or quasi-planar (2D) in the small size regime with the appearance of three-dimensional (3D) borospherene cages of larger sizes. A seashell-like B_{28}^- cluster was previously shown to be the smallest borospherene, which competes with a quasi-planar isomer for the global minimum. Here we report a study on the structures and bonding of the B_{29}^- and B_{29} clusters using photoelectron spectroscopy (PES) and first-principles calculations and demonstrate the continued competition between the 2D and borospherene structures. The PES spectrum of B_{29}^- displays a complex pattern with evidence of low-lying isomers. Global-minimum searches and extensive theoretical calculations revealed a complicated potential energy surface for B_{29}^- with five low-lying isomers, among which the lowest three were shown to contribute to the experimental spectrum. A 3D seashell-like C_s (**2**, $^1A'$) isomer, featuring two heptagons on the waist and one octagon at the bottom, is the global minimum for B_{29}^-, followed by a 2D C_1 (**3**, ^1A) isomer with a hexagonal hole and a stingray-shaped 2D C_s (**1**, $^1A'$) isomer with a pentagonal hole. However, by taking into account the entropic effects, the stingray-shaped isomer **1** was shown to be the lowest in energy at room temperature and was found to dominate the PES spectrum. Isomers **2** and **3**, which have lower electron binding energies, were also found to be present in the experiment. Chemical bonding analyses showed that isomer **1** is an all-boron analogue of benzo[*ghi*]fluoranthene ($C_{18}H_{10}$), whereas the borospherene isomer **2** possesses 18π electrons, conforming to the $2(N + 1)^2$ electron counting rule for spherical aromaticity. For the B_{29} neutral cluster, the seashell-like borospherene isomer is the global minimum, significantly lower in energy than the stingray-shaped quasi-planar structure.

1. Introduction

Boron is a prototypical electron-deficient element and forms strong covalent bonds with itself and with other elements. However, unlike its neighbor carbon, boron sheets with a honeycomb lattice are unstable because of the electron deficiency. Bulk boron is dominated by icosahedral B_{12} building blocks covalently bonded to each other, and boranes and many boron alloys also possess three-dimensional (3D), cage-like structural units. Over the past decade, a large body of experimental and theoretical works[1–21] has unraveled the structural evolution of anionic boron clusters up to B_{28}^-, which have all been found to possess unique planar or quasi-planar (2D) structures as their global minima. Beyond B_{28}^-, a number of larger clusters, such as B_n^- (n = 30, 35, 36, 39, 40), have also been also elucidated,[13,14,22–25] extending the 2D boron clusters to as large as B_{36}^-.[23,24]

All 2D B_n^- clusters are shown to consist of a periphery and one or more interior atoms. The periphery of all the 2D boron clusters is bonded by classical two-center two-electron (2c-2e)

[a] *Nanocluster Laboratory, Institute of Molecular Science, Shanxi University, Taiyuan 030006, China. E-mail: hj.zhai@sxu.edu.cn, lisidian@sxu.edu.cn*
[b] *Department of Chemistry, Brown University, Providence, Rhode Island 02912, USA. E-mail: lai-sheng_wang@brown.edu*
[c] *Institute of Materials Science, Xinzhou Teachers' University, Xinzhou 034000, China*
[d] *State Key Laboratory of Quantum Optics and Quantum Optics Devices, Shanxi University, Taiyuan 030006, China*

† Electronic supplementary information (ESI) available: Alternative optimized low-lying structures of B_{29}^- within 1 eV of the global minimum at the PBE0/6-311+G* level, along with the relative energies for top five lowest-energy structures at the single-point CCSD(T) level (Fig. S1); simulated photoelectron spectra for the fourth and fifth isomers of B_{29}^- (Fig. S2); a comparison of the simulated photoelectron spectra for top three isomers using two theoretical methods (Fig. S3); an alternative version of the bonding patterns of quasi-planar C_s B_{29}^- and C_{2v} $C_{18}H_{10}$ as revealed from adaptive natural density partitioning (AdNDP), with the Clar type π bonds (Fig. S4); comparisons of experimental VDEs of B_{29}^- with those calculated at time-dependent PBE0/6-311+G* and ROVGF/6-311+G* levels for isomers **1–5** (Table S1); and Cartesian coordinates of top three isomers of B_{29}^- at the PBE0/6-311+G* level (Table S2). See DOI: 10.1039/c6cp05420j

B–B σ bonds, whereas delocalized bonding (both π and σ) is found in the interior of the 2D boron clusters, giving rise to the concepts of aromaticity and antiaromaticity in boron clusters.[6,7,11,12,21] On the basis of π bonding, a close analogy has been established between 2D boron clusters and polycyclic aromatic hydrocarbons (PAHs).[8,9,12–14,26–29] The interior of the 2D boron clusters is mainly composed of B_3 triangles, decorated by tetragonal, pentagonal, or hexagonal holes. For example, the B_n^- (n = 20, 21, 23–28) series of clusters[10,15–19] were shown to contain one or two pentagonal holes, whereas B_{30}^-, B_{35}^-, and B_{36}^- all contain hexagonal holes. The discovery of the 2D B_{36} cluster with a central hexagonal hole provided the first indirect evidence of the viability of 2D boron monolayers, dubbed borophene.[23] The subsequent finding of the B_{35}^- cluster with two adjacent hexagonal holes provided an even more flexible building block for borophenes.[13] Recently, borophenes have been synthesized on Ag substrates,[30,31] representing a milestone in boron chemistry. Another key discovery is the observation of the B_{40}^- borospherene,[14] which is the first free-standing all-boron hollow cage, analogous to the C_{60} buckyball (albeit with substantially different structures and bonding). Shortly after that, the C_3/C_2 B_{39}^- clusters were characterized as chiral borospherenes.[25] Very recently, the seashell-like C_2 B_{28}^-, which competes with the 2D C_2 B_{28}^- for the global minimum, was observed as the smallest borospherene.[19,20]

The B_{29}^- cluster has thus far eluded us, because of its rather complex PES spectra and the challenges for global optimizations. What is the global minimum structure of B_{29}^-? Is it planar? Does it possess a pentagonal or hexagonal hole? Is the seashell-like cage structure present for B_{29}^-? A computational study on B_{29}^- has appeared,[32] suggesting that its global-minimum structure is 2D with a hexagonal hole and C_1 symmetry. As our experimental and theoretical data will show, the B_{29}^- anion cluster has several competitive low-lying structures, contributing to the complicated PES spectra observed. Both a stingray-shaped 2D C_s (**1**, $^1A'$) structure and a seashell-like C_s (**2**, $^1A'$) borospherene are found to be low-lying isomers, whose relative stabilities are found to be governed by entropy. At around room temperature, the 2D isomer **1** dominates, with the borospherene isomer **2** being slightly higher in energy. However, at 0 K, **2** is calculated to be the most stable and **1** is 0.21 eV higher in energy at the PBE0 level. In between isomers **1** and **2**, there appears to be a third, 2D isomer: C_1 (**3**, ^1A). Isomers **1**, **2**, and **3** are shown to coexist in the experimental PES spectrum. For the B_{29} neutral, the seashell isomer is the most stable, with the stingray isomer being 0.90 eV higher in energy at PBE0. Bonding analyses show that **1** is an inorganic analogue of benzo[*ghi*]fluoranthene ($C_{18}H_{10}$), whereas **2** exhibits three-dimensional aromaticity, with 18π electrons conforming to the $2(N + 1)^2$ electron-counting rule for spherical aromaticity.[33]

2. Experimental and theoretical methods

2.1. Anion photoelectron spectroscopy

The photodetachment experiment of the B_{29}^- cluster was carried out using a magnetic-bottle PES apparatus equipped with a laser vaporization source, details of which can be found elsewhere.[34] Briefly, boron clusters were produced by laser vaporization of an isotopically enriched ^{10}B (96%) target. Clusters were entrained by a He carrier gas containing 5% Ar and underwent a supersonic expansion to form a collimated beam using a skimmer. The size distribution and cooling of the clusters were controlled by the time delay between the pulsed valve and the vaporization laser, as well as by the resident time of clusters in the nozzle.[35,36] Negatively charged boron clusters were extracted perpendicularly from the molecular beam and analyzed using a time-of-flight mass spectrometer. The B_{29}^- cluster was mass-selected and decelerated before being intercepted by a 193 nm (6.424 eV) laser beam from an ArF excimer laser. Photoelectrons were collected at nearly 100% efficiency by the magnetic bottle and analyzed in a 3.5 m long electron flight tube. The PES spectrum was calibrated using the known spectrum of Au^- and the resolution of the PES apparatus was $\Delta E_k/E_k \approx 2.5\%$, that is, ~25 meV for 1 eV kinetic energy electrons.

2.2. Computational methods

Global-minimum searches for the B_{29}^- cluster were accomplished using the Minima Hopping (MH) algorithm,[37] as well as the TGmin code developed based on the Basin Hopping (BH) algorithm,[22,23,38] at the density-functional theory (DFT) level. Manual structural constructions were also done based on the known planar, cage-like, and tubular boron cluster motifs to aid the structural searches. By running the MH and TGmin searches from independent initial structures, we obtained about 4100 and 1200 structures, respectively. All isomers within ~1 eV of the global minimum were reoptimized at the PBE0/6-311+G* level.[39,40] Vibrational frequencies were calculated to ensure that the reported isomeric structures are true minima on the potential energy surface. A set of five neutral B_{29} structures, which correspond to the top five lowest-lying isomers of B_{29}^-, were also optimized and calculated at the PBE0/6-311+G* level.

For more accurate assessment of the relative energies for the isomers of B_{29}^-, single-point CCSD(T)[41–43] calculations were carried out for the top five isomers with the 6-311+G* basis set, at their corresponding PBE0/6-311+G* geometries. The first vertical detachment energy (VDE) for an isomer was computed by the energy difference between the anion and the neutral at the respective anion geometry. The higher VDEs, corresponding to the excited states of the neutral, were calculated using two methods: the time-dependent DFT (TD-DFT)[44] and the outer valence Green's function (OVGF).[45–47] Bonding analyses were performed using canonical molecular orbitals (CMOs) at the PBE0/6-311+G* level, as well as adaptive natural density partitioning (AdNDP)[48] at the PBE0/6-31G level. The AdNDP results were visualized using the Molekel 5.4.0.8 program.[49] All calculations were performed using the Gaussian 09 package.[50]

3. Experimental results

The PES spectrum of B_{29}^- at 193 nm is shown in Fig. 1(a). It displays a complex spectral pattern with reasonably well-defined

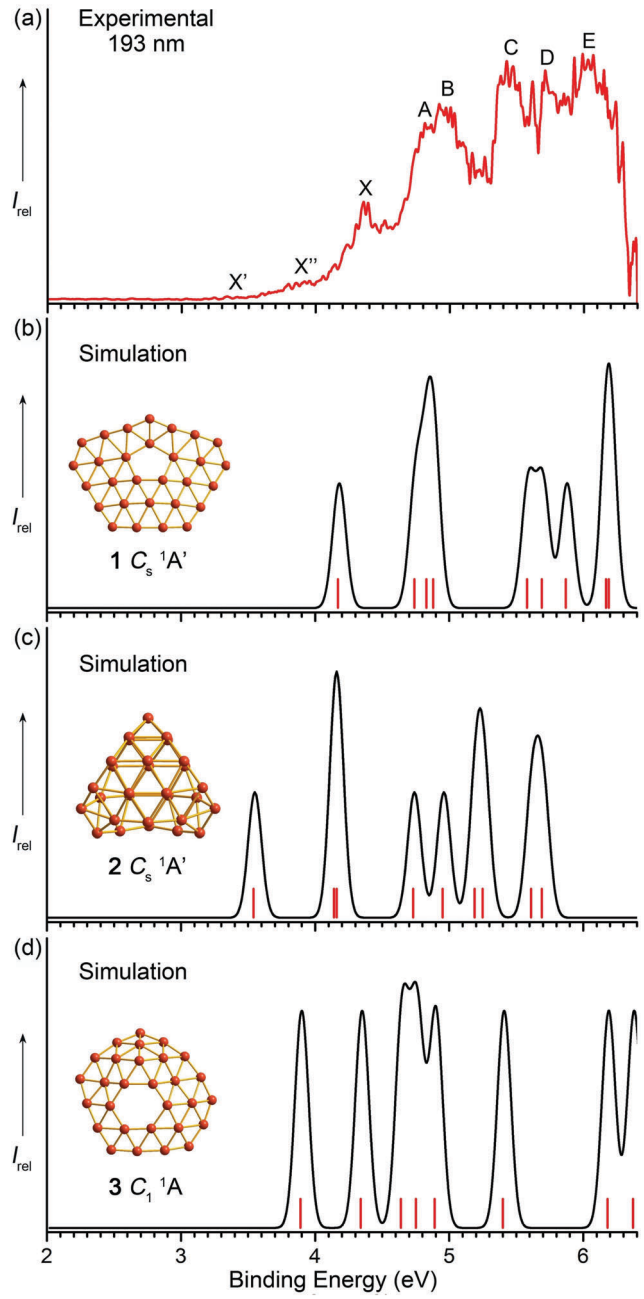

Fig. 1 Photoelectron spectrum of B_{29}^- at 193 nm (a) and comparison with simulated spectra of isomers **1** (b), **2** (c), and **3** (d) at the time-dependent PBE0/6-311+G* (TD-PBE0) level. The simulations were done by fitting the calculated VDEs (vertical bars), with unit-area Gaussian functions of 0.05 eV half-width. I_{rel} represents the relative intensity.

spectral features beyond 4.2 eV, labeled as X and A–E. The spectrum also shows a long, low binding energy tail down to ~3.2 eV. These weak signals could be due to vibrational hot bands, but the extent of the energy range of these weak signals suggests that they are most likely due to contributions from weakly populated low-lying isomers. Band X should correspond to the transition from the ground state of (the dominant isomer of) B_{29}^- to that of the corresponding neutral B_{29}, with a VDE of 4.37 ± 0.03 eV. This VDE value is quite high for boron clusters beyond n = 24,[21] suggesting that B_{29}^- is closed-shell. Since no vibrational structure is resolved for band X, the adiabatic detachment energy (ADE) is estimated by drawing a straight line along the leading edge of band X and then adding the experimental resolution to the intersection with the binding energy axis. The ADE so evaluated is 4.15 ± 0.05 eV, which also represents the electron affinity (EA) of the corresponding neutral B_{29} cluster. Among the low binding energy weak signals originated from minor isomers, two bands are tentatively labeled, X′ (~3.4 eV) and X″ (~3.9 eV), for the sake of discussion. The measured VDEs for B_{29}^- are collected in Table S1 in the (ESI†), where they are compared with the computational data.

Band A corresponds to the first excited state of neutral B_{29} associated with the main anion isomer. Band A with a VDE at 4.84 eV is separated from band X by an energy gap of 0.47 eV. Band B at a VDE of 4.97 eV is overlapped with band A. Band C is measured with a VDE of 5.44 eV, following an energy gap of 0.47 eV from band B. Beyond band C, two additional bands D (5.70 eV) and E (6.04 eV) are labeled. All the observed PES bands are broad, due to either large geometric changes between the anion and the neutral, or multiple detachment transitions.

4. Theoretical results

4.1. Global minimum searches for B_{29}^-

The MH and BH searches for B_{29}^-, in combination with manual structural constructions, generated about 5300 stationary points on the potential energy surface. The reoptimized low-lying structures at the PBE0/6-311+G* level are presented in the ESI† (Fig. S1). As many as 97 structures were identified within 1 eV of the global minimum, about 25 of them being within 0.5 eV. The top five isomers were further refined at the single-point CCSD(T) level. The low-lying isomers of B_{29}^- are dominated by 2D structures, although a couple of 3D cage-like structures are also observed to be among the low-lying isomers.

The top five lowest-lying isomers of B_{29}^- at the PBE0 and single-point CCSD(T) levels are shown in Fig. 2(a), along with the relative energies at CCSD(T) with corrections for Gibbs free energies at 298 K. These isomers are labeled as **1**, **2**, **3**, **4**, and **5**, according to their Gibbs free energies at room temperature. Isomers **1**, **2**, and **3** are essentially degenerate at room temperature, which are critical for the interpretation of the experiment at finite temperatures. At 298 K, isomers **1**–**5** span a narrow energy range of 0.11 eV, and none could be ruled out without comparison with the experiment.

Note that the energy order of the isomers varies at the PBE0 and single-point CCSD(T) levels (at 0 K). Both levels of theory indicate that isomer **2** is the global minimum, followed by **3**. Isomer **1** is predicted to be 0.21 and 0.13 eV higher in energy at PBE0 and CCSD(T), respectively. The global minimum reported previously[32] corresponds to isomer **4** (C_1, ^{1}A), which occurs as the fourth low-lying isomer at both levels of theory, even with consideration of the entropic effect.

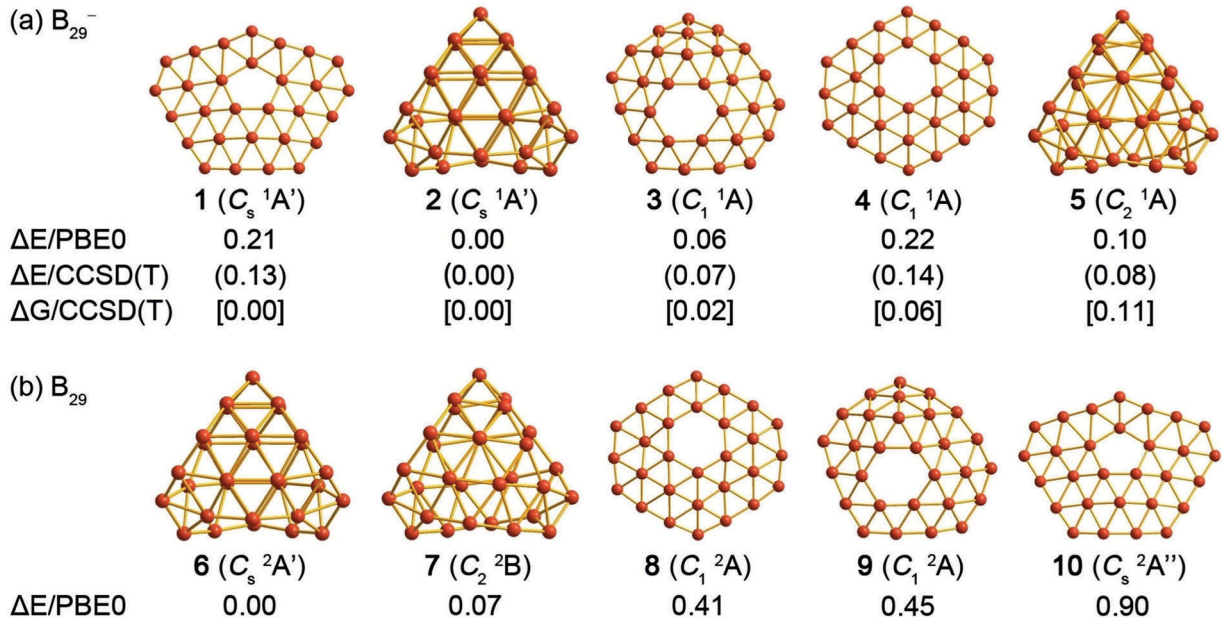

Fig. 2 The top five lowest-lying structures (**1–5**) for B_{29}^- at the PBE0/6-311+G* level, along with their relative energies (in eV) at three levels of theory: PBE0/6-311+G*, single-point CCSD(T) at PBE0/6-311+G* geometries (in parentheses), and CCSD(T) with corrections for Gibbs free energies at 298 K (in square brackets). The PBE0 and CCSD(T) data are corrected for zero-point energies at PBE0. Gibbs free energies are calculated at the PBE0/6-311+G* level. The same set of low-lying isomers for B_{29} (**6–10**) at the PBE0 level are also shown.

4.2. The top five lowest-lying structures of B_{29}^-

Isomer **1** (C_s, ^{1}A′) is quasi-planar with a central pentagonal hole. It has a stingray-like shape with an out-of-plane distortion of 2.15 Å. Isomer **1** may be constructed from the seventh isomer of the B_{30}^- cluster[22] *via* the removal of one B atom from a hexagon, or from the ninth isomer of the B_{28}^- cluster[19] by inserting one B atom into the heptagon. Isomer **2** (C_s, ^{1}A′) is a seashell-like cage, similar to the seashell B_{28}^- borospherene.[19] It consists of two quasi-planar B_{15} triangular sheets, being fused together by sharing one apex atom at the top and forming two B_2 interlaces at the bottom. Isomer **2** has two heptagons on the waist and one octagon at the bottom. The overall dimensions of the B_{29}^- seashell are 3.95, 6.13, and 5.65 Å, for its thickness, length, and width, respectively. Isomer **3** (C_1, ^{1}A) is also quasi-planar, containing a hexagonal hole and a filled pentacoordinate B atom. The Cartesian coordinates of the three lowest-lying structures (**1–3**) are given in Table S2 (ESI†).

Isomer **4** is also quasi-planar (C_1), featuring a hexagonal hole. Isomer **5** is another seashell-like structure, differing from isomer **2** by the orientation of the two B_2 interlaces. Isomer **4** was reported in a recent theoretical study as the global minimum for B_{29}^-,[32] whereas isomers **1–3** and **5** were not reported previously.

4.3. The B_{29} neutral cluster

For the neutral B_{29} cluster, the same set of five isomers corresponding to the anion isomers **1–5** are optimized at the PBE0/6-311+G* level, as shown in Fig. 2(b) (**6–10**). The energetic order of the neutral isomers differs from that of the anion at the PBE0 level of theory. Apparently, both seashell-like isomers **6** (C_s, ^{2}A′) and **7** (C_2, ^{2}B) are favored in the neutral, while the 2D structures become notably higher in energy. In particular, the stingray-like isomer **10**, which corresponds to the anion isomer **1**, becomes 0.90 eV higher in energy for the neutral ion.

5. Discussion

5.1. Comparison between experiment and theory and the effects of finite temperatures

We calculated the VDEs for isomers **1–5** of the B_{29}^- cluster using TD-DFT and compared the simulated PES spectra with the experimental data. The simulated PES spectra of isomers **1**, **2**, and **3**, obtained by fitting unit Gaussians of width 0.05 eV to the computed VDEs, are compared with the measured PES spectrum in Fig. 1. Isomers **1–3** give distinct first VDEs of 4.17, 3.54, and 3.89 eV, respectively, at the PBE0 level. The computed first VDE of 4.17 eV for isomer **1** agrees well with the experimental band X. The computed ADE, or EA, of 4.06 eV for isomer **1** is also in excellent agreement with the measured ADE for band X (4.15 ± 0.05 eV). Furthermore, the higher VDE bands in the simulated spectrum of isomer **1** are also consistent with the major observed PES bands. In particular, the observed energy gaps between bands X and A, as well as between bands B and C, are well reproduced in the simulated spectrum of isomer **1**.

The lower first VDEs for isomers **2** (3.54 eV) and **3** (3.89 eV) are consistent with the observed weak low binding energy features of X′ (~3.4 eV) and X″ (~3.9 eV), respectively, suggesting that isomers **2** and **3** are weakly populated in the B_{29}^- cluster beam. The simulated spectra for isomers **4** and **5** are given in Fig. S2 (ESI†). The two isomers also have low first VDEs.

While their contributions to the extended low binding energy tail in the experimental spectrum cannot be completely ruled out, populations of these isomers are expected to be minimal, if any.

To further confirm the simulated PES spectra at the TD-PBE0 level, we also computed the VDEs for isomers **1–3** using OVGF, as compared with the PBE0 results in Fig. S3 (ESI†). The OVGF data are generally similar to those of TD-PBE0. Overall, the theoretical results are in good agreement with the experimental observation, lending considerable credence for the identified global minimum and low-lying isomers for B_{29}^-.

Clearly, temperature plays an important role in the relative population of the isomers. Isomer **1** is not the global minimum at 0 K. But its Gibbs free energy becomes the lowest at about room temperature (Fig. 3). Even though the temperature of the clusters is not known exactly in the experiment, our previous experience suggests that clusters in this size range should be at about room temperature or sub-room temperature.[35,36] Fig. 3 shows the relative Gibbs free energies for the top five isomers as a function of temperature. At 0 K, the seashell isomer **2** is the lowest in energy, followed by the quasi-planar **3** and seashell-like **5** at 0.07 and 0.08 eV, respectively, as also shown in Fig. 2(a). With increasing temperature, the Gibbs free energy of the seashell isomer **5** increases slightly relative to that of isomer **2**, whereas those for isomers **1**, **3**, and **4** all decrease. In particular, the stingray isomer **1** displays the sharpest drop. Thus, at room temperature, isomers **1–3** become virtually isoenergetic, in agreement with their coexistence experimentally. The Gibbs free energy curves in Fig. 3 predict the region where isomers **1–3** may coexist and reproduce the observed relative distributions. Considering the uncertainty of the computational methods in terms of energetics, we think that the prediction (300 K or slightly larger) is quite good in comparison to the experiment (around room temperature, or slightly lower).[35,36]

5.2. The stingray-shaped C_s (1) isomer of B_{29}^- as an analogue of benzo[*ghi*]fluoranthene

The chemical bonding in the stingray-shaped isomer **1** is analyzed using both the CMOs and the AdNDP approach. Since this C_s isomer is quasi-planar, we flatten it to a planar C_{2v} species in the chemical bonding analyses in order to gain a clearer view of the σ and π bonding. The CMOs of isomer **1** show nine completely delocalized π bonds (Fig. 4(a)), suggesting an aromatic π system.[51] More interestingly, we have found that the π bonding in isomer **1** is analogous to that in benzo[*ghi*]fluoranthene ($C_{18}H_{10}$), as shown in Fig. 4(b). The π CMOs in the two systems exhibit remarkable similarities, suggesting that the stingray-like C_s (**1**) isomer of B_{29}^- can be considered as an all-boron analogue of $C_{18}H_{10}$.

Alternatively, the bonding in the C_s B_{29}^- (**1**) and benzo[*ghi*]-fluoranthene may be understood on the basis of AdNDP analyses.[48] In AdNDP, the bonding of a molecular system is represented in terms of *n*-center two-electron (*n*c-2e) bonds, with the value of *n* ranging from one to the total number of atoms in the system. AdNDP thus recovers not only the classical Lewis elements (lone-pairs and 2c-2e bonds), but also delocalized multi-center bonds.

Even though the solutions from AdNDP are not unique, one guiding principle for the bonding analyses should be to obtain a chemically intuitive bonding picture for such a complex cluster system. Our AdNDP results for C_s B_{29}^- (**1**) are presented in Fig. 5(a). There are thirty-six B_3 triangles and one pentagon in B_{29}^-, with forty-four pairs of valence electrons. For the σ framework, we find the familiar 2c-2e σ bonds for the seventeen peripheral B–B bonds, as well as five 3c-2e σ bonds around

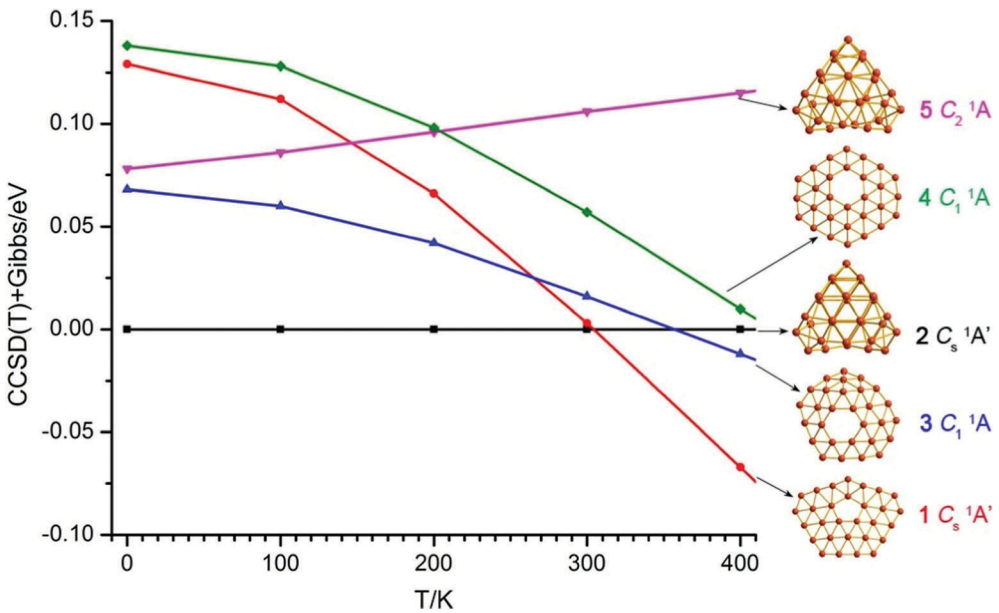

Fig. 3 Relative energies of the top five isomers (**1–5**) of B_{29}^- at the single-point CCSD(T) level, with Gibbs free energy corrections at PBE0/6-311+G* as a function of temperature from 0 to 400 K. The energies are plotted relative to that of the seashell-like C_s (**2**) structure.

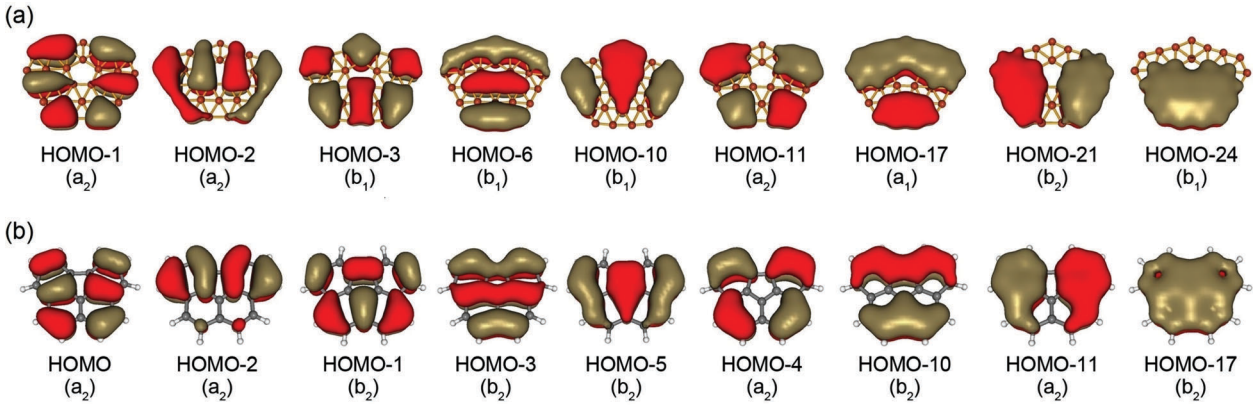

Fig. 4 Comparison of the π canonical molecular orbitals (CMOs) of (a) the flattened C_s (**1**) B_{29}^- cluster and (b) the benzo[*ghi*]fluoranthene ($C_{18}H_{10}$) PAH.

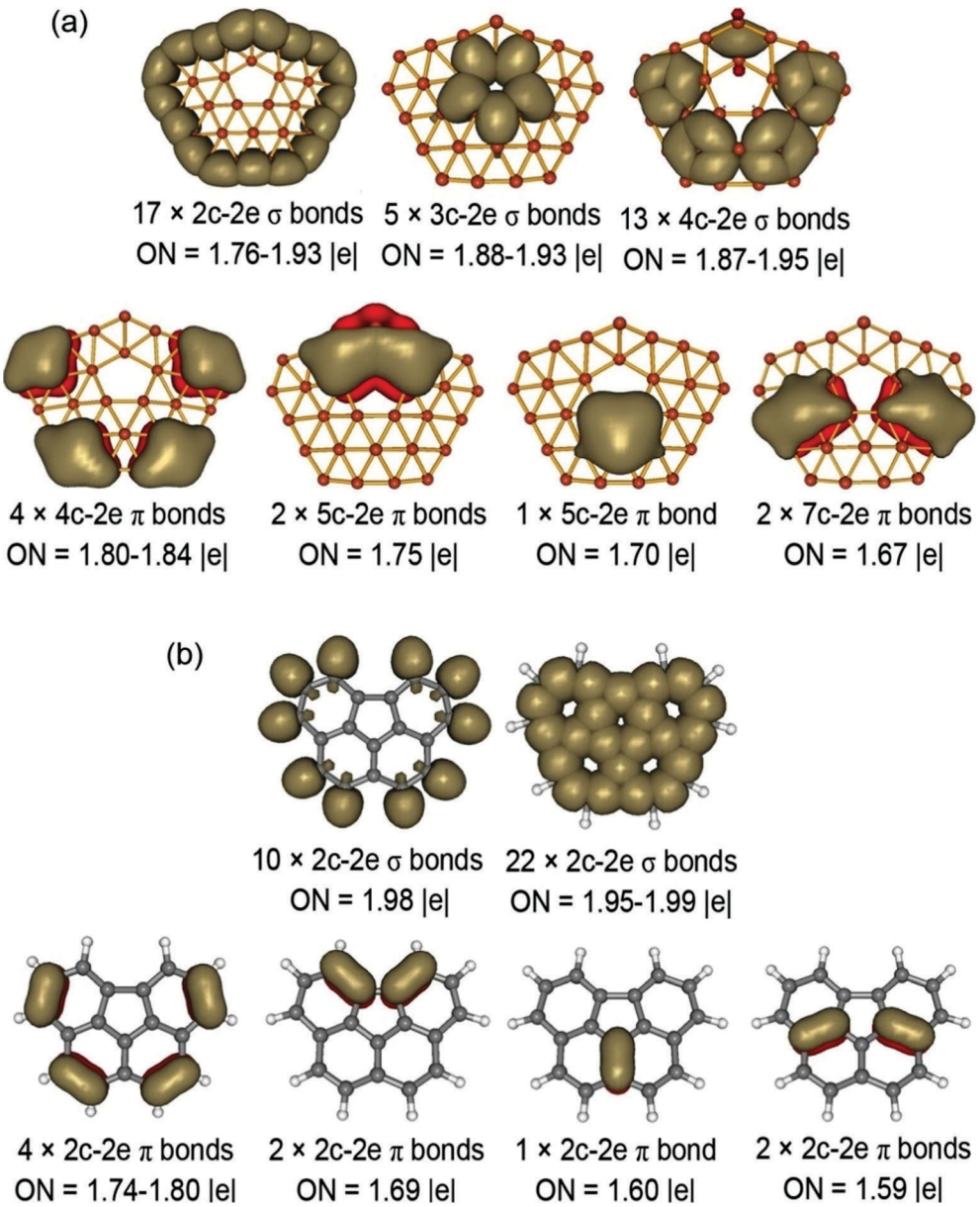

Fig. 5 Results of AdNDP bonding analyses for (a) the C_s (**1**) isomer of B_{29}^- and (b) the $C_{18}H_{10}$ PAH at the PBE0/6-31G level. Occupation numbers (ONs) are shown.

the inner B_5 hole and thirteen 4c-2e σ bonds. As anticipated, the nine π CMOs of C_s B_{29}^- (**1**) have been transformed into nine delocalized π bonds: four 4c-2e, three 5c-2e, and two 7c-2e π bonds (Fig. 5a, second row). This π bonding scheme is referred to as being of the Kekule type. A similar bonding analysis for benzo[*ghi*]fluoranthene is shown in Fig. 5(b), again demonstrating the close analogy between the π bonding in the C_s B_{29}^- (**1**) and benzo[*ghi*]fluoranthene. π bonding can also be represented in the Clar-type schemes, as shown in Fig. S4 (ESI†) for the C_s B_{29}^- (**1**) and benzo[*ghi*]fluoranthene, which also reveals the analogy in π bonding between the two systems.

5.3. Chemical bonding in the seashell-like C_s (2) borospherene of B_{29}^-

The bonding in the seashell-like B_{29}^- C_s (**2**) isomer was analyzed *via* AdNDP only, because the CMOs are simply too complicated for the low symmetry 3D species. The AdNDP results are shown in Fig. 6. The C_s (**2**) borospherene has thirty-eight B_3 triangles, of which sixteen are on each B_{15} sheet and six are situated at the interface of the two B_{15} sheets (two for each of the three corners). The AdNDP analyses give rise to thirty-four 3c-2e σ bonds, plus one 6c-2e σ bond involving two B_3 triangles on the two B_{15} sheets. The σ framework involves thirty-five delocalized σ bonds, leaving eighteen electrons for the π framework.

π bonding is relatively simple (Fig. 6, second row): each B_{15} sheet has three 5c-2e π bonds, and the remaining three π bonds are situated at the three corners, involving both B_{15} sheets. Note that all the σ and π bonds in the B_{29}^- borospherene are delocalized, similar to the B_{40} borospherene.[14] The 18π electrons in B_{29}^- also conform to the $2(N + 1)^2$ electron counting rule for spherical aromaticity ($N = 2$). Indeed, the calculated nuclear independent chemical shift (NICS)[52] at the cage center is −21.27 ppm at the PBE0/6-311+G* level, which is highly negative, and consistent with spherical aromaticity.

Finally, it should be pointed out that different isomer ordering between the B_{29}^- anion and the B_{29} neutral is similar to that observed previously for B_{40}^-/B_{40} and B_{28}^-/B_{28}.[14,19] In each case, reordering is related to the EA of a given isomer, which determines the stability of the anion. In the case of B_{40}^-, the extremely low EA of the cage isomer makes the borospherene anion less stable relative to the planar one. In the case of B_{29}^-, the calculated EA of 4.06 eV for **1** is much higher than the value of 3.37 eV for **2** at the PBE0 level. Consequently, upon detachment of the extra electron from the anions, the stingray-shaped neutral isomer (**10**) becomes substantially destabilized with respect to the seashell isomer (**6**).

6. Conclusions

In conclusion, we have studied the structures and chemical bonding of the B_{29}^- cluster using anion photoelectron spectroscopy and quantum chemical calculations and found a rather complicated potential landscape for the medium-sized boron cluster. A quasi-planar stingray-shaped C_s (**1**) isomer and a seashell-like borospherene C_s (**2**) isomer are shown to be nearly degenerate and are observed to coexist in the size-selected anion PES experiment. The third quasi-planar C_1 (**3**) isomer is also low in energy and makes minor contributions to the observed PES spectrum. Entropies are shown to be important for determining the relative stabilities of different isomers at finite temperatures. While at 0 K isomer **2** is the most stable, followed by **3** and **1**, with increasing temperature isomer **1** becomes more stable with respect to **2** and is the major isomer observed experimentally. For neutral B_{29}, the seashell borospherene isomer

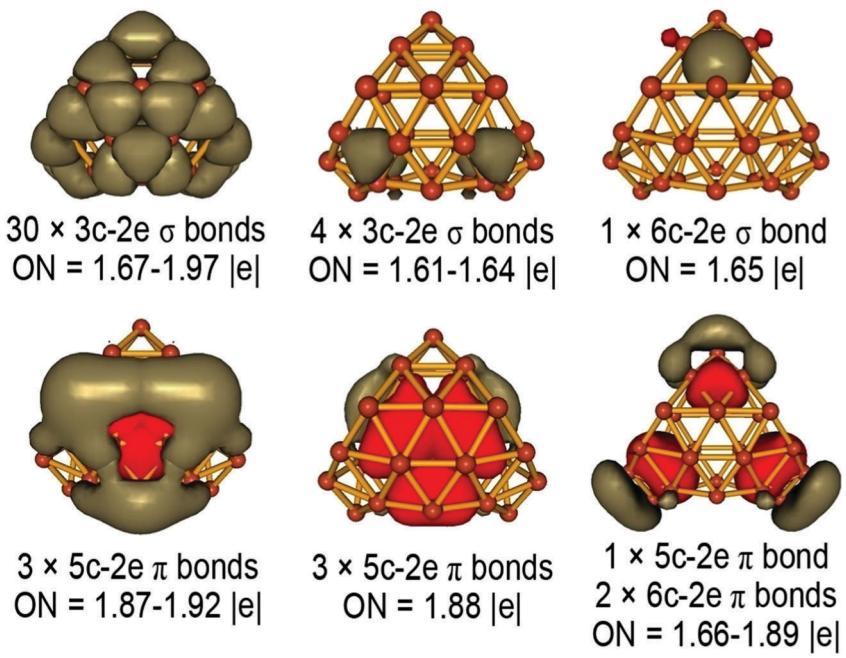

Fig. 6 Results of AdNDP bonding analyses for the seashell-like C_s (**2**) isomer of B_{29}^-. Occupation numbers (ONs) are shown.

is the global minimum and the stingray-shaped isomer becomes a higher energy species. Chemical bonding analyses reveal that the quasi-planar C_s B_{29}^- (**1**), featuring nine delocalized π bonds, is an all-boron analogue of benzo[*ghi*]fluoranthene ($C_{18}H_{10}$). The seashell-like C_s B_{29}^- (**2**) represents a new member of the borospherene family. All its σ and π bonds are delocalized and its 18π electrons conform to the $2(N + 1)^2$ electron-counting rule for spherical aromaticity.

Acknowledgements

The experimental work done at Brown University was supported by the US National Science Foundation (CHE-1632813). The theoretical work was supported by the National Natural Science Foundation of China (21573138, 21373130) and the State Key Laboratory of Quantum Optics and Quantum Optics Devices (KF201402).

Notes and references

1 L. Hanley, J. L. Whitten and S. L. Anderson, *J. Phys. Chem.*, 1988, **92**, 5803.
2 E. Oger, N. R. M. Crawford, R. Kelting, P. Weis, M. M. Kappes and R. Ahlrichs, *Angew. Chem., Int. Ed.*, 2007, **46**, 8503.
3 J. I. Aihara, H. Kanno and T. Ishida, *J. Am. Chem. Soc.*, 2005, **127**, 13324.
4 J. E. Fowler and J. M. Ugalde, *J. Phys. Chem. A*, 2000, **104**, 397.
5 I. Boustani, *Int. J. Quantum Chem.*, 1994, **52**, 1081.
6 A. N. Alexandrova, A. I. Boldyrev, H. J. Zhai and L. S. Wang, *Coord. Chem. Rev.*, 2006, **250**, 2811.
7 A. P. Sergeeva, I. A. Popov, Z. A. Piazza, W. L. Li, C. Romanescu, L. S. Wang and A. I. Boldyrev, *Acc. Chem. Res.*, 2014, **47**, 1349.
8 H. J. Zhai, A. N. Alexandrova, K. A. Birch, A. I. Boldyrev and L. S. Wang, *Angew. Chem., Int. Ed.*, 2003, **42**, 6004.
9 H. J. Zhai, B. Kiran, J. Li and L. S. Wang, *Nat. Mater.*, 2003, **2**, 827.
10 B. Kiran, S. Bulusu, H. J. Zhai, S. Yoo, X. C. Zeng and L. S. Wang, *Proc. Natl. Acad. Sci. U. S. A.*, 2005, **102**, 961.
11 A. P. Sergeeva, D. Yu. Zubarev, H. J. Zhai, A. I. Boldyrev and L. S. Wang, *J. Am. Chem. Soc.*, 2008, **130**, 7244.
12 W. Huang, A. P. Sergeeva, H. J. Zhai, B. B. Averkiev, L. S. Wang and A. I. Boldyrev, *Nat. Chem.*, 2010, **2**, 202.
13 W. L. Li, Q. Chen, W. J. Tian, H. Bai, Y. F. Zhao, H. S. Hu, J. Li, H. J. Zhai, S. D. Li and L. S. Wang, *J. Am. Chem. Soc.*, 2014, **136**, 12257.
14 H. J. Zhai, Y. F. Zhao, W. L. Li, Q. Chen, H. Bai, H. S. Hu, Z. A. Piazza, W. J. Tian, H. G. Lu, Y. B. Wu, Y. W. Mu, G. F. Wei, Z. P. Liu, J. Li, S. D. Li and L. S. Wang, *Nat. Chem.*, 2014, **6**, 727.
15 Z. A. Piazza, W. L. Li, C. Romanescu, A. P. Sergeeva, L. S. Wang and A. I. Boldyrev, *J. Chem. Phys.*, 2012, **136**, 104310.
16 A. P. Sergeeva, Z. A. Piazza, C. Romanescu, W. L. Li, A. I. Boldyrev and L. S. Wang, *J. Am. Chem. Soc.*, 2012, **134**, 18065.
17 Z. A. Piazza, I. A. Popov, W. L. Li, R. Pal, X. C. Zeng, A. I. Boldyrev and L. S. Wang, *J. Chem. Phys.*, 2014, **141**, 034303.
18 W. L. Li, R. Pal, Z. A. Piazza, X. C. Zeng and L. S. Wang, *J. Chem. Phys.*, 2015, **142**, 204305.
19 Y. J. Wang, Y. F. Zhao, W. L. Li, T. Jian, Q. Chen, X. R. You, T. Ou, X. Y. Zhao, H. J. Zhai, S. D. Li, J. Li and L. S. Wang, *J. Chem. Phys.*, 2016, **144**, 064307.
20 J. J. Zhao, X. M. Huang, R. L. Shi, H. S. Liu, Y. Su and R. B. King, *Nanoscale*, 2015, **7**, 15086.
21 L. S. Wang, *Int. Rev. Phys. Chem.*, 2016, **35**, 69.
22 W. L. Li, Y. F. Zhao, H. S. Hu, J. Li and L. S. Wang, *Angew. Chem., Int. Ed.*, 2014, **53**, 5540.
23 Z. A. Piazza, H. S. Hu, W. L. Li, Y. F. Zhao, J. Li and L. S. Wang, *Nat. Commun.*, 2014, **5**, 3113.
24 Q. Chen, G. F. Wei, W. J. Tian, H. Bai, Z. P. Liu, H. J. Zhai and S. D. Li, *Phys. Chem. Chem. Phys.*, 2014, **16**, 18282.
25 Q. Chen, W. L. Li, Y. F. Zhao, S. Y. Zhang, H. S. Hu, H. Bai, H. R. Li, W. J. Tian, H. G. Lu, H. J. Zhai, S. D. Li, J. Li and L. S. Wang, *ACS Nano*, 2015, **9**, 754.
26 H. J. Zhai, Q. Chen, H. Bai, S. D. Li and L. S. Wang, *Acc. Chem. Res.*, 2014, **47**, 2435.
27 H. J. Zhai, S. D. Li and L. S. Wang, *J. Am. Chem. Soc.*, 2007, **129**, 9254.
28 S. D. Li, H. J. Zhai and L. S. Wang, *J. Am. Chem. Soc.*, 2008, **130**, 2573.
29 D. Z. Li, H. Bai, Q. Chen, H. G. Lu, H. J. Zhai and S. D. Li, *J. Chem. Phys.*, 2013, **138**, 244304.
30 A. J. Mannix, X. F. Zhou, B. Kiraly, J. D. Wood, D. Alducin, B. D. Myers, X. L. Liu, B. L. Fisher, U. Santiago, J. R. Guest, M. J. Yacaman, A. Ponce, A. R. Oganov, M. C. Hersam and N. P. Guisinger, *Science*, 2015, **350**, 1513.
31 B. J. Feng, J. Zhang, Q. Zhong, W. B. Li, S. Li, H. Li, P. Cheng, S. Meng, L. Chen and K. H. Wu, *Nat. Chem.*, 2016, **8**, 563.
32 T. B. Tai and M. T. Nguyen, *Phys. Chem. Chem. Phys.*, 2015, **17**, 13672.
33 A. Hirsch, Z. F. Chen and H. J. Jiao, *Angew. Chem., Int. Ed.*, 2000, **39**, 3915.
34 L. S. Wang, H. S. Cheng and J. W. Fan, *J. Chem. Phys.*, 1995, **102**, 9480.
35 W. Huang and L. S. Wang, *Phys. Rev. Lett.*, 2009, **102**, 153401.
36 J. Akola, M. Manninen, H. Häkkinen, U. Landman, X. Li and L. S. Wang, *Phys. Rev. B: Condens. Matter Mater. Phys.*, 1999, **60**, R11297.
37 S. Goedecker, W. Hellmann and T. Lenosky, *Phys. Rev. Lett.*, 2005, **95**, 055501.
38 D. J. Wales and H. A. Scheraga, *Science*, 1999, **285**, 1368.
39 C. Adamo and V. Barone, *J. Chem. Phys.*, 1999, **110**, 6158.
40 R. Krishnan, J. S. Binkley, R. Seeger and J. A. Pople, *J. Chem. Phys.*, 1980, **72**, 650.
41 J. Čížek, *Adv. Chem. Phys.*, 1969, **14**, 35.
42 G. D. Purvis and R. J. Bartlett, *J. Chem. Phys.*, 1982, **76**, 1910.
43 K. Raghavachari, G. W. Trucks, J. A. Pople and M. Head-Gordon, *Chem. Phys. Lett.*, 1989, **157**, 479.
44 R. Bauernschmitt and R. Ahlrichs, *Chem. Phys. Lett.*, 1996, **256**, 454.
45 W. von Niessen, J. Schirmer and L. S. Cederbaum, *Comput. Phys. Rep.*, 1984, **1**, 57.
46 V. G. Zakrzewski and J. V. Ortiz, *Int. J. Quantum Chem.*, 1995, **53**, 583.

47 J. V. Ortiz, *Adv. Quantum Chem.*, 1999, **35**, 33.
48 D. Yu. Zubarev and A. I. Boldyrev, *Phys. Chem. Chem. Phys.*, 2008, **10**, 5207.
49 U. Varetto, *Molekel 5.4.0.8*, Swiss National Supercomputing Center, Manno, Switzerland, 2009.
50 M. J. Frisch, G. W. Trucks, H. B. Schlegel, G. E. Scuseria, M. A. Robb, J. R. Cheeseman, G. Scalmani, V. Barone, B. Mennucci, G. A. Petersson, H. Nakatsuji, M. Caricato, X. Li, H. P. Hratchian, A. F. Izmaylov, J. Bloino, G. Zheng, J. L. Sonnenberg, M. Hada, M. Ehara, K. Toyota, R. Fukuda, J. Hasegawa, M. Ishida, T. Nakajima, Y. Honda, O. Kitao, H. Nakai, T. Vreven, J. A. Montgomery, Jr., J. E. Peralta, F. Ogliaro, M. Bearpark, J. J. Heyd, E. Brothers, K. N. Kudin, V. N. Staroverov, R. Kobayashi, J. Normand, K. Raghavachari, A. Rendell, J. C. Burant, S. S. Iyengar, J. Tomasi, M. Cossi, N. Rega, J. M. Millam, M. Klene, J. E. Knox, J. B. Cross, V. Bakken, C. Adamo, J. Jaramillo, R. Gomperts, R. E. Stratmann, O. Yazyev, A. J. Austin, R. Cammi, C. Pomelli, J. W. Ochterski, R. L. Martin, K. Morokuma, V. G. Zakrzewski, G. A. Voth, P. Salvador, J. J. Dannenberg, S. Dapprich, A. D. Daniels, Ö. Farkas, J. B. Foresman, J. V. Ortiz, J. Cioslowski and D. J. Fox, *GAUSSIAN 09, Revision D.01*, Gaussian, Inc., Wallingford, CT, 2009.
51 Even though the $(4n + 2)$ Hückel rule was for aromaticity in *monocyclic* hydrocarbon molecules, it has been found that many planar boron clusters can be considered as aromatic using this electron counting rule, by comparison with analogous hydrocarbons. In the current case, the π bonding in isomer **1** of the B_{29}^- cluster is found to be analogous to that in the polycyclic aromatic hydrocarbon, benzo[*ghi*]fluoranthene. The aromaticity in isomer **1** is probably weakened due to the out-of-plane distortion.
52 P. v. R. Schleyer, C. Maerker, A. Dransfeld, H. J. Jiao and N. J. v. E. Hommes, *J. Am. Chem. Soc.*, 1996, **118**, 6317.